

2D GaN for Highly Reproducible Surface Enhanced Raman Scattering

Shasha Zhao, Huiliu Wang, Lixin Niu, Wenqi Xiong, Yunxu Chen, Mengqi Zeng, Shengjun Yuan, and Lei Fu*

Surface-enhanced Raman scattering (SERS) based on 2D semiconductors has been rapidly developed due to their chemical stability and molecule-specific SERS activity. High signal reproducibility is urgently required towards practical SERS applications. 2D gallium nitride (GaN) with highly polar Ga–N bonds enables strong dipole–dipole interactions with the probe molecules, and abundant DOS (density of states) near its Fermi level increases the intermolecular charge transfer probability, making it a suitable SERS substrate. Herein, 2D micrometer-sized GaN crystals are demonstrated to be sensitive SERS platforms with excellent signal reproducibility and stability. Strong dipole–dipole interaction between the dye molecule and 2D GaN enhances the molecular polarizability. Furthermore, 2D GaN benefits its SERS enhancement by the combination of increased DOS and more efficient charge transfer resonances when compared with its bulk counterpart.

1. Introduction

Surface-enhanced Raman scattering (SERS) is a rapid, sensitive, and nondestructive technology to detect chemical and biological compounds through unique vibrational fingerprints.^[1–5] SERS based on semiconductors has been rapidly developed for chemical stability and molecule-specific SERS activity.^[6] When semiconductors come to two dimensions, they exhibit the surface with a large specific surface area, and coordination number of the surface atoms is insufficient for their easy adsorption with molecules to form complexes. Hence, 2D semiconductors are suitable for fundamental studies and practical applications of the SERS effect.^[6–13] The Raman enhancement of 2D semiconductors depends on their distinct electronic structures and surface chemical properties,^[7] and derives from charge-transfer, excitonic, and molecular resonance.^[14] The Raman enhancement effects are mainly contributed by electronic tran-

sitions between 2D semiconductors and probe molecules. Electron transition probability during the charge-transfer process can be expressed by Fermi's golden rule

$$w_{ik} = \frac{2\pi}{\hbar} |H_{ki}'|^2 g(E_k),$$

where w_{ik} is the charge transition probability, H_{ki}' is the matrix element of the highest-occupied molecular orbital (HOMO)–lowest-unoccupied molecular orbital (LUMO) transition, \hbar is the reduced Planck constant, and $g(E_k)$ is density of states (DOS) of the final state.^[10,12] Relatively small band gap and high DOS enable strong vibronic coupling in ultrathin amorphous TiO₂, thus enhancing charge-transfer resonance.^[12]

Surface defect sites in WO₃ nanosheets increase charge-carrier density and induce strong charge transfer at the substrate-molecule interface, thus improving sensitivity of the substrate.^[13] Enhanced charge-transfer and exciton resonances in the vertical heterostructure ReO_xS_y/graphene improved sensitivity of the substrate as well.^[11]

III–V semiconductors are potential in high-speed, high-frequency electronics, and high-efficiency optoelectronics for their high charge carrier mobility,^[15] efficient light detection,^[16] and emission.^[17] Unique characteristics emerge in their 2D form,^[18–22] promoting their property exploration in the 2D limit.^[23] The research on chemical mechanism of SERS can be achieved by using III–V semiconductors as SERS substrates, excluding surface plasmon resonance (SPR) as the origin of Raman enhancement. In addition, current state-of-art semiconductor technology can be utilized to prepare III–V semiconductor substrates with good reproducibility and low cost. The biocompatibility of III–V semiconductors such as gallium nitride (GaN)^[24] together with easy and highly reproducible fabrication process endow them as promising SERS substrates with wide applicability.

When comes to 2D the surface activity of GaN increases, thus facilitating the adsorption of molecules on its surface (Figure 1a).^[25] Furthermore, owing to the electronegativity difference between the Ga (1.76) and N (3.07) atoms^[26], 2D GaN shows a highly polarized surface profile (Figure S1, Supporting Information) and its highly polar Ga–N bonds enable dipole–dipole interactions with the probe molecules, inducing local symmetry-related perturbations that increase the matrix element,^[11] thus increasing the electron transition probability.^[14] Furthermore, we calculated the DOS of 2D GaN

S. S. Zhao, H. L. Wang, L. X. Niu, Y. X. Chen, M. Q. Zeng, L. Fu
College of Chemistry and Molecular Sciences
Wuhan University
Wuhan 430072, China
E-mail: leifu@whu.edu.cn

W. Q. Xiong, S. J. Yuan
School of Physics and Technology
Wuhan University
Wuhan 430072, China

 The ORCID identification number(s) for the author(s) of this article can be found under <https://doi.org/10.1002/sml.202103442>.

DOI: 10.1002/sml.202103442

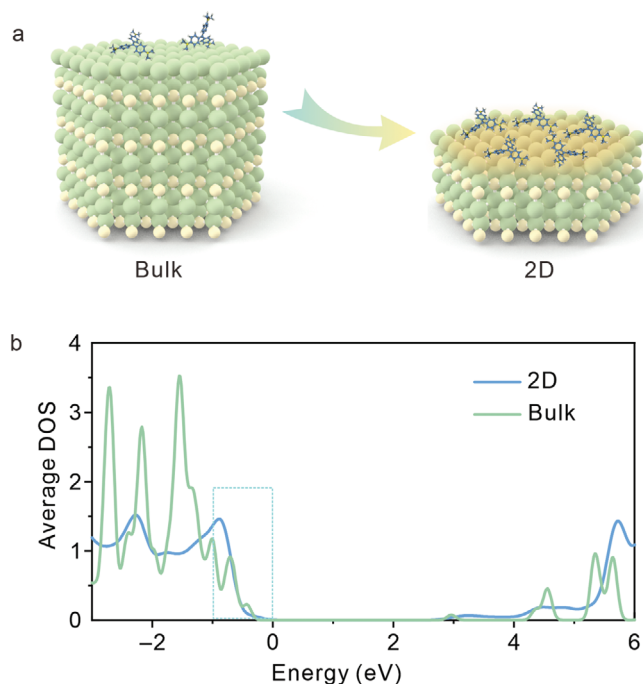


Figure 1. a) Illustration of structure transition of GaN from bulk to 2D form, indicating the facilitated adsorption of molecules. b) The DOS of bulk and 2D GaN near the Fermi level.

and bulk GaN (for details see Section S2, Figures S2 and S3 in the Supporting Information) to investigate the charge transfer probability between the molecule and GaN. 2D GaN has abundant DOS near the Fermi level, increasing the intermolecular charge transfer probability as well (Figure 1b). Therefore, 2D GaN is expected to be a proper SERS substrate. Herein, we have investigated the SERS effects of 2D GaN. They exhibit SERS sensitivity down to 10^{-7} M for dye molecule with high signal reproducibility (relative standard deviation, RSD of 9.09%). Density functional theory (DFT) calculation results illustrate that a large number of charges transfer from the adsorbed molecule to 2D GaN, forming a stable complex and increasing the molecular polarizability. Furthermore, excellent SERS performance of 2D GaN is achieved by increasing photo-induced charge transfer (PICT) pathways and promoting the charge transfer resonances in the analyte-substrate complex.

2. Results and Discussion

High-quality 2D GaN flakes with lateral size of ≈ 40 μm were grown on liquid metal gallium in chemical vapor deposition (CVD) process (Section S1, Supporting Information).^[20] Figures S4 and S5 in the Supporting Information confirm hexagon morphology of the crystals. Energy dispersive spectroscopy (EDS) elemental mapping indicates that N and Ga element are uniformly distributed in the crystal. An exclusive peak 566.2 cm^{-1} (E_2 longitudinal optical mode) in the Raman spectrum of 2D GaN confirms its fabrication (Figure 2a). This main Raman signature is away from the Raman-active region of most common dye analytes (600 – 1800 cm^{-1}), which can largely avoid the unwanted Raman interference in SERS demonstra-

tion. Atomic force microscopy (AFM) characterization was conducted to identify the thickness of 2D GaN. Its thickness is 24.1 nm (Figure 2b).

To evaluate the SERS performance of the 2D crystal, a typical dye molecule, crystal violet (CV) was utilized as the Raman probe, a prohibited fish drug, which may pose health risks and adverse environmental impact. The wavelength-dependent SERS measurements of CV molecule on 2D GaN were carried out. Raman spectra of CV on 2D GaN in Figure S6 (Supporting Information) exhibit obvious signals under the 532 nm excitation, while weak SERS signals are observed under the 633 nm excitation and no SERS signal is observed under the 785 nm excitation. CV is a typical fluorescent molecule, its HOMO–LUMO gap (1.70 eV) is close to the energy of the excitation wavelength 633 nm (1.96 eV). Under the 633 nm excitation, immense fluorescence background overwhelms the Raman signals. Furthermore, the CV solution (2×10^{-4} M) was drop-casted on GaN and the Raman spectra under the 532 nm excitation taken from regions of bulk, 2D GaN, and SiO_2/Si substrate covered by CV molecules are exhibited in Figure 2c. It is demonstrated that stronger SERS effect occurs on the 2D GaN crystal than those on bulk GaN and SiO_2/Si (Figure 2c; Table S1, Supporting Information).

SERS performance is of great interest for probing trace amounts of molecules. A series of CV solutions were prepared (Figure S7, Supporting Information) to investigate the SERS sensitivity of 2D GaN. Conspicuous Raman signatures of CV appear in the Raman spectra of CV/2D GaN with various concentrations (Figure 2d). The fingerprint Raman bands were still detectable at 2×10^{-7} M (Figure S8, Supporting Information), enabling 2D GaN to be a sensitive SERS platform. The corresponding Raman enhancement factor was 5.2×10^5 taking bulk probe molecule as the reference (Figure S9, Section S3, and Table S2, Supporting Information).

Besides the enhancement magnitude, reproducibility is additional important criterium in evaluating SERS substrates. To investigate the SERS signal reproducibility of GaN, 30 randomly chosen points on bulk and 2D GaN were tested, respectively. The SERS signal intensity from the 2D mapping of 2×10^{-4} M CV on 2D GaN in Figure 3a demonstrates uniform SERS signals induced by the 2D crystal. Furthermore, the relative standard deviation (RSD) of signal intensities obtained from 30 spots on 2D and bulk GaN for detecting CV solution (2×10^{-4} M) have been calculated, respectively. Signal reproducibility on the 2D crystal is significantly improved (9.09%, Figure 3b), while the bulk crystal shows weak and nonreproducible SERS performance (80.88%, Figures S10, Supporting Information). The high SERS signal reproducibility of dye molecules on 2D GaN is due to a relatively strong and uniform interaction between the analytes and the surface of 2D GaN. In contrast, bulk GaN crystals which expose various crystal facets (Figure S11, Supporting Information), result in facet-dependent work functions, thereby changing interfacial charge transfer and leading to non-uniform SERS performance.^[27] The crystal structure of 2D GaN has not been modified by the CV adsorption, as demonstrated in the Raman spectra of 2D GaN in Figure S12 in the Supporting Information. SERS stability is also essential for a feasible SERS substrate toward practical applications. The SERS intensity of 2D GaN was well maintained without significant variations, even after its exposure

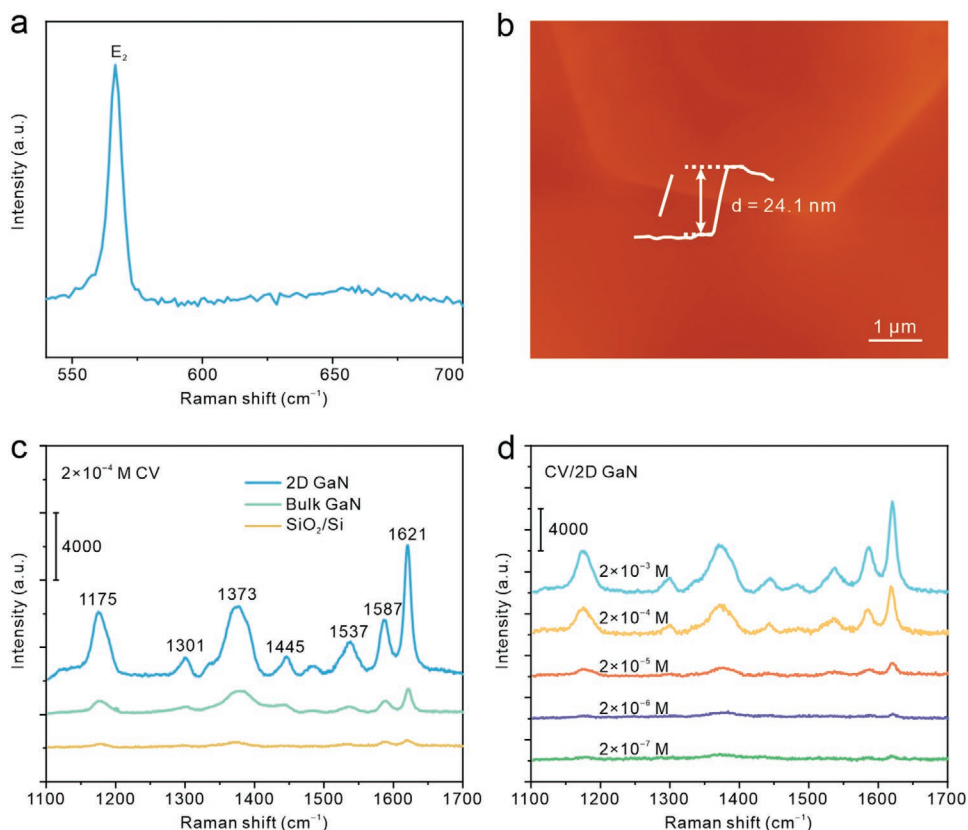


Figure 2. a) Raman spectrum of 2D GaN. b) AFM image of 2D GaN. c) Raman spectra of CV on SiO₂/Si, bulk and 2D GaN. d) Raman spectra of CV solution on 2D GaN with various concentrations.

to ambient air conditions for 60 d (Figure 3c,d), evidencing its reliable SERS effect against air exposure. The high SERS stability of CV on 2D GaN was attributed to the satisfactory air stability of 2D GaN (Figure S13, Supporting Information) as well as the robust adsorption of the probe molecules on 2D GaN. Furthermore, we have conducted measurements on the photostability of SERS spectra of CV/2D GaN (2×10^{-4} M). The decrease of Raman intensity of dye molecules on 2D GaN is limited (Figure S14, Supporting Information), indicating large charge transfer between the molecule and substrate, which provides additional path for the dye molecules to relax from excitation state to ground state, and hence reduce the probability of photoreaction for the molecules at excitation states.^[28]

Another interesting topic is to discuss the influence of the thickness of 2D GaN on the Raman enhancement effect. Figure S15 (Supporting Information) gives the Raman spectra of CV (2×10^{-4} M) on 2D GaN having various thicknesses. As its thickness increases, Raman signal intensity of CV molecule dramatically decreases. The thickness dependent SERS performance is mainly attributed to photoinduced charge transfer process.^[29] The thickness-dependent bandstructure of 2D GaN, and the chemisorption capability of the crystal with different thicknesses, may also contribute to the total Raman enhancement.^[9]

The SERS effect on 2D GaN is a universal phenomenon for a diverse range of dyes, such as methylene blue (MB), rhodamine 6G (R6G), and *p*-dimethylaminobenzaldehyde (PDAB). As shown in Figure S16a and Table S3 (Supporting Information), the prominent signal of MB (1×10^{-4} M) peak are much

stronger on 2D GaN than that on SiO₂/Si. Raman peaks of MB can still be observed at 1×10^{-6} M (Figure S16b, Supporting Information). Besides, we have tried R6G as the probe molecule, and found that stronger peaks occurred in the Raman spectrum of R6G coated on 2D GaN than that on SiO₂/Si under the 532 nm excitation (Figure S16c and Table S4, Supporting Information). As for PDAB, a nonresonant organic molecule, Raman intensity of PDAB on 2D GaN^[30,31] is stronger than that on SiO₂/Si (Figure S16d and Table S5, Supporting Information). Considering that the HOMO–LUMO bandgap of PDAB is 4.3 eV,^[32] much larger than 2.33 eV (532 nm excitation wavelength), therefore, in PDAB/2D GaN system, there is no molecular resonance under the 532 nm excitation, indicating that charge transfer in this system has played a significant role in enhanced Raman intensity.

To have a comprehensive understanding of the rationale for excellent SERS activity of 2D GaN, systematic investigations have been conducted. Notably, the electromagnetic enhancement (EM) contribution was excluded in the GaN-induced SERS effect, since its SPR wavelength is at the far-infrared regime (Section S4, Supporting Information). Based on the above reasoning, we demonstrate that the enhanced Raman spectrum of dye molecules on GaN stems from chemical enhancement mechanism.

DFT calculations were performed to provide an in-depth understanding of chemical mechanism of the SERS effect (for details see Section S2, Supporting Information). To investigate the interfacial charge transfer between CV and 2D GaN, the

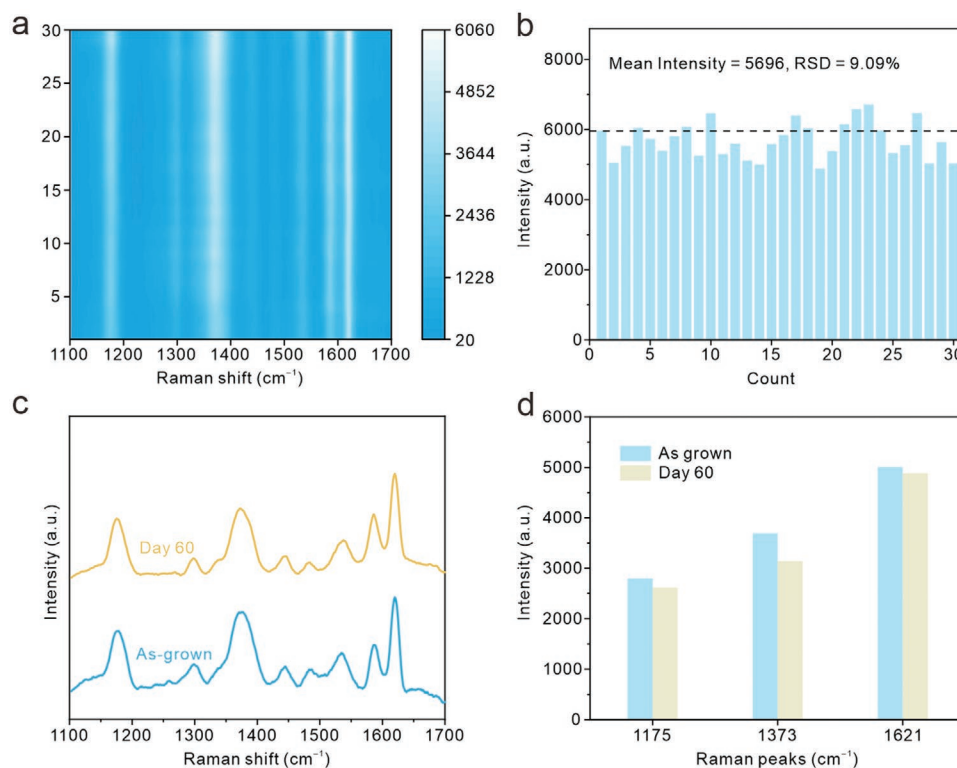


Figure 3. a) 2D mapping of Raman intensity of CV (2×10^{-4} M) on 2D GaN with 30 randomly selected points for the research of signal uniformity. b) Peak intensity of the 1621 cm^{-1} line in the Raman spectrum of CV (2×10^{-4} M) on 2D GaN from these points. c) Evolution of Raman spectra of CV (2×10^{-4} M) on 2D GaN after aging in ambient for up to 60 d. d) Raman intensity of CV 1175 , 1373 , and 1621 cm^{-1} peak on CV/2D GaN as the function of storage time in air. The data were extracted from (c).

charge difference distribution for CV/2D GaN system was calculated. According to the calculation results, the electron transferred from the dye molecule to 2D GaN was $0.63 e/\text{molecule}$ (Figure 4a). Furthermore, it is found that for the CV/2D GaN system, the electrons and holes generated by charge transfer were closely located around the surface of the crystal, and the CV molecule, respectively, forming a dipole at the interface. As a result, the SERS effect of the CV molecule on the 2D GaN crystal was prompted. Furthermore, the isotropic polarizabilities of CV molecule and CV/2D GaN system were calculated to analyze the contribution of charge transfer to the molecular polarizability, revealing that 2D GaN could cause amplification of the molecular polarization (Table S6, Supporting Information, CV: $554.34 \text{ Bohr}^3/\text{atom}$, CV/2D GaN: $658.51 \text{ Bohr}^3/\text{atom}$). Therefore, 2D GaN effectively caused the interfacial charge transfer and thus magnified the molecular polarization. The dipole between the dye molecule and the substrate brought about the excellent SERS performance of 2D GaN.

In addition to the static coupling of the probe molecule and SERS substrate, strong SERS effect on 2D GaN originates from the PICT driven chemical mechanism. As we have mentioned that the electron transition probability during the charge-transfer process is closely related with the DOS near the Fermi level. It is demonstrated from the DOS of GaN near the Fermi level (Figure 1b) that 2D GaN possessed more electronic states and the electron transition probability was increased, thus it gave better Raman enhancement, consistent with our results. Furthermore, we have conducted a series of band structure analysis between the substrate and molecule. First, the valence

band of 2D GaN near the Fermi level, which has been measured via valence-band XPS (X-ray photoelectron spectroscopy) (Figure S17, Supporting Information) was 3.94 eV . Second, its work function was determined by Kelvin probe force microscopy (KPFM). According to the surface potential image of 2D GaN in Figure S18, Supporting Information, its work function was 4.08 eV (Section S5, Supporting Information). Furthermore, the bandgap of 2D GaN was 3.48 eV , according to the UV-vis absorption spectrum (Figure S19, Supporting Information). Based on these characterizations, the conduction band minimum (CBM) and valence band maximum (VBM) of 2D GaN were -4.54 and -8.02 eV below the vacuum level, respectively. For bulk GaN, its CBM and VBM were -3.28 and -6.64 eV below the vacuum level, respectively.^[33] Energy-level diagrams can be constructed for bulk and 2D GaN with respect to the molecule levels of CV, respectively. Two types of allowed charge transfer transitions can be inferred for the substrate-molecule systems in Figure 4b, including PICT between the substrate and molecule, and molecular transitions (μ_{IK}) between the HOMO and LUMO of CV.

The HOMO (ground state, $|I\rangle$) and LUMO (excited state, $|K\rangle$) levels of CV were -4.3 and -6.0 eV , respectively.^[34] According to Albrecht and Lombardi's theory on Raman intensity,^[14,35-37] the Raman polarization tensor α can be expressed as $\alpha = A + B + C$, where A term is relevant to the resonance Raman scattering. In CV/2D GaN system, the resonance Raman scattering could be achieved when the laser excitation energy (2.33 eV) is close to the molecular transitions (μ_{IK}) between the HOMO and LUMO of CV (1.70 eV), which contributes to the overall

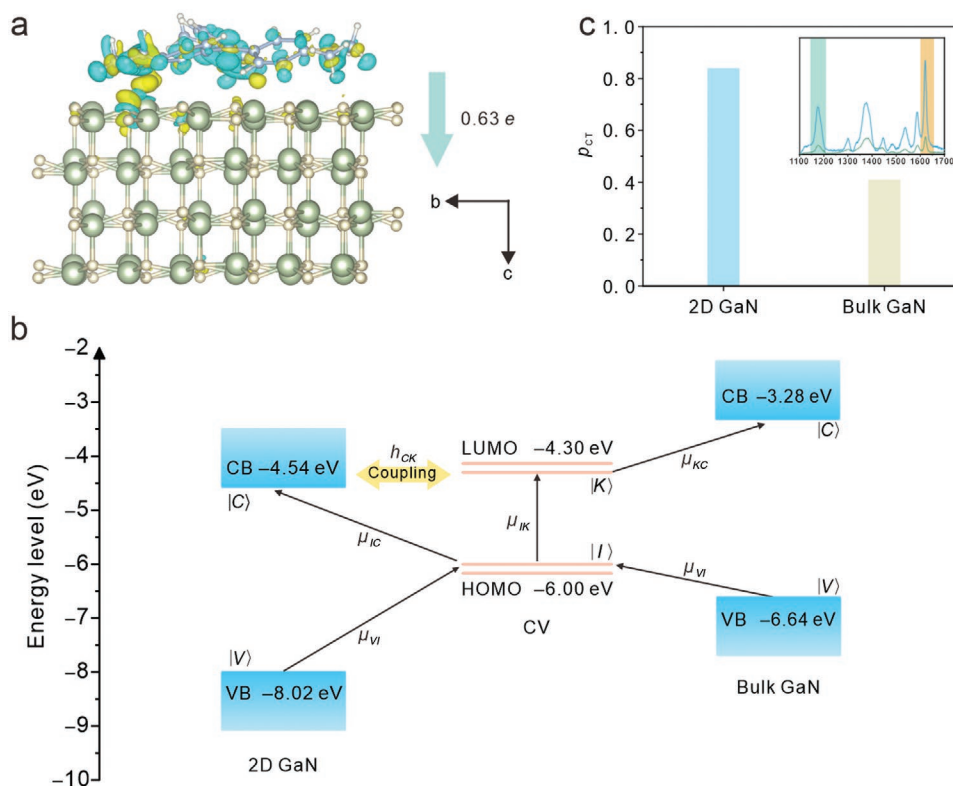


Figure 4. Chemical mechanism of the SERS effect. a) Side view of the electron density difference isosurfaces for CV on 2D GaN. Green and yellow correspond to electron depletion and accumulation regions, respectively. The electron transfer direction is indicated by the arrow. b) Band energy alignment diagram comparing the charge-transfer pathways in CV/2D GaN and CV/bulk GaN, respectively. c) Degree of charge-transfer P_{CT} for CV detected on 2D and bulk GaN. The inset shows the selective enhancement of 1175 and 1621 cm^{-1} peaks on 2D and bulk GaN.

SERS performances. As shown in Figure 4b, although the existence of molecular transitions (μ_{IK}) may provide similar SERS enhancements for CV/2D GaN and CV/bulk GaN, the distinct band structures of 2D GaN and bulk GaN cause quite different contributions to SERS based on the PICT transitions between the substrate and the molecule. For CV/bulk GaN system, two PICT processes from VB of bulk GaN to HOMO of CV (μ_{VI}) and from LUMO of CV to CB of bulk GaN (μ_{KC}) occur. Energies of these PICT processes (0.64 and 1.02 eV) were much lower than the laser photo energy at 532 nm (2.33 eV) and contributed little to the SERS performance. In contrast, in the CV/2D GaN system, two PICT processes from VB of 2D GaN to HOMO of CV (μ_{VI} , 2.02 eV), HOMO of CV to CB of 2D GaN (μ_{IC} , 1.46 eV) occur. Furthermore, energy of PICT from VB of 2D GaN to HOMO of CV (μ_{VI} , 2.02 eV) is close to the laser photo energy at 532 nm (2.33 eV), which favored the efficient PICT between CV and 2D GaN, contributing to the SERS performance. Moreover, the efficiency of PICT transition in the CV/2D GaN system strongly depended on the intensity of vibronic coupling between the CB of 2D GaN and the LUMO of CV molecule as their energy levels were coupled. In the CV/2D GaN system, PICT transition from HOMO of CV to the CB of 2D GaN via the transition moment, μ_{IC} , can borrow intensity from molecular transitions, μ_{IK} , through the Herzberg-Teller coupling term (h_{CK}).^[38] Consequently, the 2D GaN exhibits much stronger SERS activity than the bulk GaN. In summary, better Raman enhancement of dye molecules on 2D GaN in comparison with bulk GaN arises from synergistic effect of

strong dye molecule-substrate coupling and more efficient charge-transfer resonances.

Furthermore, the respective charge-transfer-contribution of 2D and bulk GaN to the SERS signal of CV was quantifiably

obtained by using the relationship $P_{CTk} = \frac{I^k(CT) - I^k(SPR)}{I^k(CT) + I^0(SPR)}$,^[39-41]

where the non-totally symmetric 1175 cm^{-1} mode was chosen as line k and the totally symmetric 1621 cm^{-1} mode was chosen as line 0. The degree of charge transfer for CV (2×10^{-4} M) on the 2D crystal was 0.87, higher than 0.46 on the bulk crystal (Figure 4c; Table S7, Supporting Information), indicating enhanced charge transfer contribution to the overall SERS detection in CV/2D GaN.

3. Conclusion

In summary, the downsizing of GaN crystals induces changes in their electronic structure to maintain thermodynamic stability within the 2D crystal. The 2D crystals exhibit high SERS reproducibility and stability. The chemical mechanism of remarkable SERS performances of 2D crystals has been investigated through theoretical calculations in combination with experimental results. The static coupling between dye molecule and the 2D crystal, increased DOS near the Fermi level as well as enhanced charge transfer resonances lead to sensitive SERS detection of dye molecules. 2D GaN is introduced for SERS

detection, enriching the diversity of SERS-active substrates, providing new insights into chemical mechanism-based charge transfer processes.

Supporting Information

Supporting Information is available from the Wiley Online Library or from the author.

Acknowledgements

S.S.Z. H.L.W., and L.X.N. contributed equally to this work. The authors thank the group of Prof. H.X.X. for Raman Spectra measurements. This work was supported by the National Natural Science Foundation of China (Grant Nos. 22025303 and 21905210), and the Sino-German Center for Research Promotion (Grant No. GZ 1400).

Conflict of Interest

The authors declare no conflict of interest.

Data Availability Statement

The data that support the findings of this study are available from the corresponding author upon reasonable request.

Keywords

2D materials, charge transfer, gallium nitride, semiconductor, surface-enhanced Raman scattering

Received: June 13, 2021

Revised: July 20, 2021

Published online:

- [1] S. M. Nie, S. R. Emory, *Science* **1997**, 275, 1102.
- [2] K. Kneipp, Y. Wang, H. Kneipp, L. T. Perelman, I. Itzkan, R. R. Dasari, M. S. Feld, *Phys. Rev. Lett.* **1997**, 78, 1667.
- [3] S. Schlücker, *Angew. Chem. Int. Ed.* **2014**, 53, 4756.
- [4] C. Zong, M. X. Xu, L.-J. Xu, T. Wei, X. Ma, X.-S. Zheng, R. Hu, B. Ren, *Chem. Rev.* **2018**, 118, 4946.
- [5] S. E. J. Bell, G. Charron, E. Cortés, J. Kneipp, M. L. Chapelle, J. Langer, M. Procházka, V. Tran, S. Schlücker, *Angew. Chem. Int. Ed.* **2020**, 59, 5454.
- [6] X. T. Wang, L. Guo, *Angew. Chem. Int. Ed.* **2020**, 59, 4231.
- [7] X. Ling, W. J. Fang, Y.-H. Lee, P. T. Araujo, X. Zhang, J. F. Rodriguez-Nieva, Y. X. Lin, J. Zhang, J. Kong, M. S. Dresselhaus, *Nano Lett.* **2014**, 14, 3033.
- [8] Y. Yin, P. Miao, Y. M. Zhang, J. C. Han, X. H. Zhang, Y. Gong, L. Gu, C. Y. Xu, T. Yao, P. Xu, Y. Wang, B. Song, S. Jin, *Adv. Funct. Mater.* **2017**, 27, 1606694.
- [9] L. Tao, K. Chen, Z. Chen, C. Cong, C. Qiu, J. Chen, X. Wang, H. Chen, T. Yu, W. Xie, S. Deng, J. Xu, *J. Am. Chem. Soc.* **2018**, 140, 8696.
- [10] X. J. Song, Y. Wang, F. Zhao, Q. C. Li, H. Q. Ta, M. H. Ruemmeli, C. G. Tully, Z. Z. Li, W.-J. Yin, L. T. Yang, K.-B. Lee, J. Yang, I. Bozkurt, S. W. Liu, W. J. Zhang, M. Chhowalla, *ACS Nano* **2019**, 13, 8312.
- [11] J. Seo, J. Lee, Y. Kim, D. Koo, G. Lee, H. Park, *Nano Lett.* **2020**, 20, 1620.
- [12] X. Wang, W. Shi, S. Wang, H. Zhao, J. Lin, Z. Yang, M. Chen, L. Guo, *J. Am. Chem. Soc.* **2019**, 141, 5856.
- [13] G. Song, W. B. Gong, S. Cong, Z. G. Zhao, *Angew. Chem. Int. Ed.* **2021**, 60, 5505.
- [14] I. Alessandri, J. R. Lombardi, *Chem. Rev.* **2016**, 116, 14921.
- [15] J. A. Alamo, *Nature* **2011**, 479, 317.
- [16] J. F. Wang, M. S. Gudiksen, X. F. Duan, Y. Cui, C. M. Lieber, *Science* **2001**, 293, 1455.
- [17] Y. Kim, S. S. Cruz, K. Lee, B. O. Alawode, C. Choi, Y. Song, J. M. Johnson, C. Heidelberger, W. Kong, S. Choi, K. Qiao, I. Almansouri, E. A. Fitzgerald, J. Kong, A. M. Kolpak, J. Hwang, J. Kim, *Nature* **2017**, 544, 340.
- [18] A. V. Kolobov, P. Fons, J. Tominaga, B. Hyot, B. Andre, *Nano Lett.* **2016**, 16, 4849.
- [19] Z. Z. Qin, G. Z. Qin, X. Zuo, Z. H. Xiong, M. Hu, *Nanoscale* **2017**, 9, 4295.
- [20] Y. X. Chen, K. L. Liu, J. X. Liu, T. R. Lv, B. Wei, T. Zhang, M. Q. Zeng, Z. C. Wang, L. Fu, *J. Am. Chem. Soc.* **2018**, 140, 16392.
- [21] Z. Y. A. Balushi, K. Wang, R. K. Ghosh, R. A. Vila, S. M. Eichfeld, J. D. Caldwell, X. Y. Qin, Y.-C. Lin, P. A. DeSario, G. Stone, S. Subramanian, D. F. Paul, R. M. Wallace, S. Datta, J. M. Redwing, J. A. Robinson, *Nat. Mater.* **2016**, 15, 1166.
- [22] N. Sanders, D. Bayerl, G. S. Shi, K. A. Mengle, E. Kioupakis, *Nano Lett.* **2017**, 17, 7345.
- [23] Y. X. Chen, J. X. Liu, K. L. Liu, J. J. Si, Y. R. Ding, L. Y. Li, T. R. Lv, J. P. Liu, L. Fu, *Mater. Sci. Eng. R* **2019**, 138, 60.
- [24] S. A. Jewett, M. S. Makowski, B. Andrews, M. J. Manfra, A. Ivanisevic, *Acta Biomater.* **2012**, 8, 728.
- [25] N. Zhou, R. S. Yang, T. Y. Zhai, *Mater. Today Nano* **2019**, 8, 100051.
- [26] J. B. Mann, T. L. Meek, L. C. Allen, *J. Am. Chem. Soc.* **2000**, 122, 2780.
- [27] J. Lin, W. Hao, Y. Shang, X. T. Wang, D. L. Qiu, G. S. Ma, C. Chen, S. Z. Li, L. Guo, *Small* **2018**, 14, 1703274.
- [28] Y. D. Zhao, Y. Z. Xie, Z. Y. Bao, Y. H. Tsang, L. M. Xie, Y. Chai, *J. Phys. Chem. C* **2014**, 118, 11827.
- [29] Y. Lee, H. Kim, J. Lee, S. H. Yu, E. Hwang, C. Lee, J.-H. Ahn, J. H. Cho, *Chem. Mater.* **2016**, 28, 180.
- [30] F. Y. Wang, X. L. Gu, C. C. Zheng, F. Dong, L. Y. Zhang, Y. Q. Cai, Z. Y. You, J. H. You, S. H. Du, Z. P. Zhang, *Anal. Chem.* **2017**, 89, 8836.
- [31] N. F. L. Machado, M. P. M. Marques, L. A. E. Batista de Carvalho, J. L. Castro, J. C. Otero, *J. Raman Spectrosc.* **2017**, 48, 413.
- [32] M. Rocha, A. D. Santo, J. M. Arias, D. M. Gil, A. B. Altabef, *Spectrochim. Acta, Part A* **2015**, 136, 635.
- [33] Z. F. Zhang, Q. K. , Q. B. K. Li, K. J. Chen, *ACS Appl. Mater. Interfaces* **2018**, 10, 17419.
- [34] R. Haldavnekar, K. Venkatakrishnan, B. Tan, *Nat. Commun.* **2018**, 9, 3065.
- [35] A. C. Albrecht, *J. Chem. Phys.* **1960**, 33, 156.
- [36] A. C. Albrecht, *J. Chem. Phys.* **1960**, 33, 169.
- [37] A. C. Albrecht, *J. Chem. Phys.* **1961**, 34, 1476.
- [38] J. R. Lombardi, R. L. Birke, *J. Phys. Chem. C* **2014**, 118, 11120.
- [39] J. R. Lombardi, R. L. Birke, *J. Phys. Chem. C* **2008**, 112, 5605.
- [40] C. Chenal, R. L. Birke, J. R. Lombardi, *ChemPhysChem* **2008**, 9, 1617.
- [41] A. P. Richter, J. R. Lombardi, B. Zhao, *J. Phys. Chem. C* **2010**, 114, 1610.